scenario and 4°C (2.4–6.4°C) under the worst scenario. The effect of cosmic ray intensity over long periods, however, could add or subtract to the global warming depending on whether the long-term variation of primary cosmic ray intensity shows a decreasing or an increasing trend. We conclude that the contribution to climate change due to the change in galactic cosmic ray intensity is quite significant and needs to be factored into the prediction of global warming and its effect on sea level raise and weather prediction.

1. Climatic Change 2007: The Physical Science Basis; Contribution of Working Group 1 to the Fourth Assessment Report of the Intergovernmental Panel on Climate Change, February 2007.
2. Svensmark, H. and Friis-Christensen, E., Variation of cosmic ray flux and global cloud coverage – a missing link in solar climate relationship. *J. Atmos. Sol. Terr. Phys.*, 1997, **59**, 1225.
3. McCracken, K. G. and Beer, J., The long-term changes in the cosmic ray intensity at earth, 1428–2005. *J. Geophys. Res.*, 2007, Under Publication.
4. McCracken, K. G., Beer, J. and McDonald, F. B., Variation in the cosmic radiation, 1890–1986 and the solar and terrestrial implications. *Adv. Space Res*., 2004, **34**, 397.
5. McCracken, K. G., High frequency of occurrence of large solar energetic particle events prior to 1958 and a possible repetition in the near future. *Space Weather*, 2007, **5**, S07004.
6. McCracken, K. G., The heliomagnetic field near earth 1428–2005. *J. Geophys. Res.*, 2007, **112**, A09106.
7. Taricco, N. *et al.*, Galactic cosmic ray flux decline and periodicities in the interplanetary space during the last 3 centuries revealed by ^{44}Ti in meteorites. *J. Geophys. Res.*, 2005, **111**, A08102.
8. Gleeson, L. J. and Axford, W. I., Solar modulation of galactic cosmic rays. *Astrophys. J.*, 1968, **154**, 1011.
9. Caballero-Lopez, R. A., Moraal, H., McCracken, K. G. and McDonald, F. B., *J. Geophys. Res*., 2004, **109**, A12002.
10. Eastwood, J. P., Balogh, A. and Dunlop, M. W., Cluster observations of the heliospheric current sheet and an associated magnetic flux rope and comparisons with ACE. *J. Geophys. Res*., 2002, **107**(A11), 1365.
11. Carslaw, K. S., Harrison, R. G. and Kirkby, J., Cosmic rays, clouds and climate. *Science*, 2002, **298**, 172.
12. Lee, S. H. *et al.*, Particle formation by ion nucleation in the upper troposphere and lower stratosphere. *Science*, 2003, **301**, 1886.
13. Veizer Jan, Celestial climate driver: a perspective from four billion years of the carbon cycle. *Geosci. Canada*, 2005, **32**, 13.
14. Ruderman, M. A. and Chamberlain, J. W., Origin of sunspot modulation of ozone – its implications for stratospheric NO injection. *Planetary Space Sci*., 1975, **23**, 247.
15. Rao, U. R., Geomagnetic field – its role in the evolution of life. *J. Br. Interplanet. Soc.*, 1981, **34**, 454.
16. Ramanathan, V., Callis, L. B. and Boughner, R. E., Sensitivity of surface temperature and atmospheric temperature to perturbations in stratospheric concentration of ozone and nitrogen dioxide. *J. Atmos. Sci*., 1976, **33**, 1092.

ACKNOWLEDGEMENTS. I thank Dr K. G. McCracken for very fruitful discussions and permission to reproduce Figure 1. I also thank Dr Jan Veizer for permission to reproduce Figure 2. I also thank Prof. S. K. Satheesh, CAOS, IISc, Bangalore, for valuable assistance in preparing this manuscript.

Received 20 September 2010; revised accepted 15 December 2010

Microstructure and growth band studies of uroliths using optical and scanning electron microscopy

Sanjay S. Kale[1], N. J. Pawar[2,3,*], D. S. Wagholikar[4] and Hema Achyuthan[5]

[1]Department of Environmental Sciences, and
[2]Department of Geology, University of Pune, Pune 411 007, India
[3]Present address: Shivaji University, Kolhapur 416 004, India
[4]Purandar Hospital, Saswad 412 301, India
[5]Department of Geology, Anna University, Chennai 600 025, India

Detailed description, analysis and interpretation of bio-mineral formations are fundamental to an understanding of their growth and origin. Study of morphology at the macro-level can be supplemented by examining the specimen under the microscope using thin sections prepared from undisturbed samples. Until recently the main emphasis in urological research on kidney stones (uroliths), has been to assist with biological interpretation using biological microscope supported by physical, X-ray diffraction (XRD), and scanning electron microscopy (SEM) studies. However, polarizing microscope studies have not been carried out to identify the mineral composition of the biologically formed uroliths. Biologically formed kidney stones offer an excellent material to study their microstructures and features under the optical microscope supplemented by SEM analyses to decipher and hierarchically understand its development of formation. In the present study thin sections of uroliths have been examined under a polarizing microscope (Nikon Eclipse E200) supported by SEM.

Keywords: Growth band, microstructure, polarizing microscope, uroliths.

UROLITHS are hard, irregular in shape, vary in size from 2 to 75 mm and are composed of calcium containing minerals, or are made up of crystals of calcium oxalate (CaC_2O_4) and calcium phosphate[1–10]. Kidney stones are formed by the urine (excreted product of blood) which is filtered out in both the kidneys by means of glomerulus's filtration (a functional unit of kidney). Uroliths can occur in any section of the urinary tract. Regardless of the specific type, uroliths occur when the urine becomes too concentrated with urolith precursors and the environmental conditions are appropriate for stone formation. Several studies have been carried out earlier to understand the urolith morphology, chemical composition using SEM and optical microscopy[4–6]. Till date no study has been conducted to observe the kidney-stone features using polarizing microscope. In the present study an attempt has been made to highlight the texture and

*For correspondence. (e-mail: njpawar@unipune.ac.in)

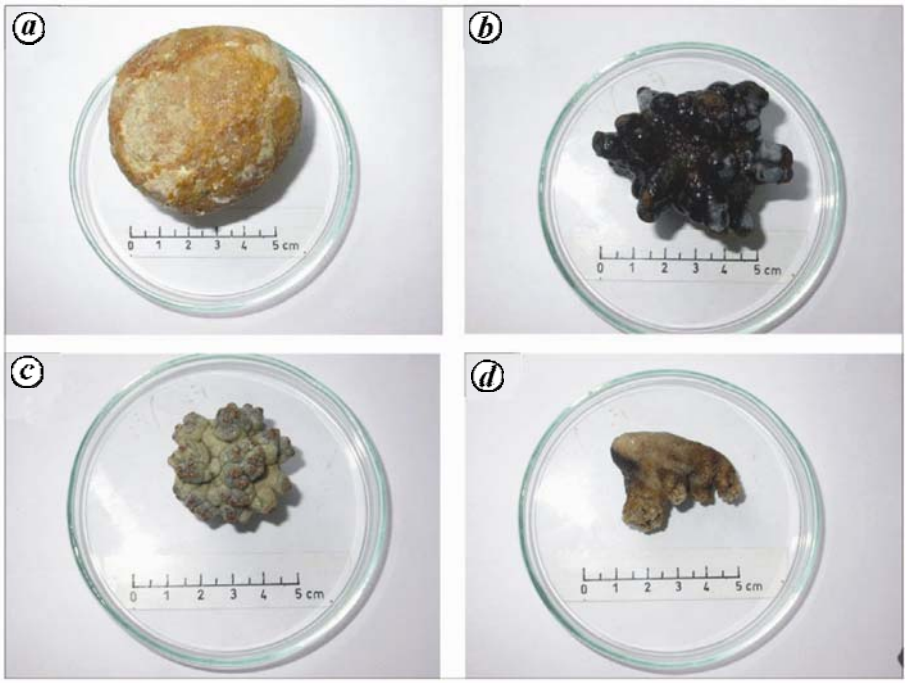

Figure 1. Representative samples of uroliths showing irregular shape and size. Samples have been obtained from hospitals in the semi-arid region, Pune District, Maharashtra. ***a–c***, Bladder stone. ***a***, Magnesium hydrogen phosphate – 25%, calcium hydrogen phosphate – 25%, ammonium hydrogen urate – 50%. ***b***, Calcium oxalate monohydrate – 10% and calcium oxalate dihydrate – 90%; ***c***, Calcium oxalate monohydrate – 80% and calcium oxalate dihydrate – 20%; ***d***, Kidney stone (calcium oxalate monohydrate – 80% and calcium oxalate dihydrate – 20%).

features of kidney stones, their shape and internal structure, location and the relationship between the crystals and the organic compounds to infer plausible causes for their formation. Nineteen urolith samples were collected from hospitals at Saswad and Baramati town, Pune District, Maharashtra, and representative kidney stones were studied (Figure 1 *a–d*). These samples were preserved in formalin solution. Outer parts were scraped using polish paper to remove impurities attached to the kidney stones. The samples were then washed with double de-ionized water to remove dirt and dust. The size of the samples collected ranges from 2 to 75 mm, and are spheroid (Figure 1 *a*), irregular, branched and papilliated (Figure 1 *b–d*). Nineteen thin sections were prepared without using the cover slip (0.5–5 μm) and using Canada Balsam (natural), and they were studied under the optical microscope and SEM[6–9]. For SEM studies, the kidney-stone samples were mounted on a brass stub, vacuum-coated with silver paste and observed under a JEOL JSM-6360 microscope at the Department of Physics, University of Pune, Pune.

The characteristic features observed were photographed and are presented in Figure 2. Cross-sections of the kidney stones under the optical polarizing microscope revealed that the CaC_2O_4 monohydrate stone shows distinct rings with radial striations surrounding a nucleus[11]. Uroliths often start with the accumulation around a nucleus that could be of organic or inorganic precipitate of CaC_2O_4 (Figure 2 *a*, *g*, *l*), or the urolith could grow over a plaque called the Randall's plaque[3]. Subsequently, concentric zones (Figure 2 *h*, *l*) accumulated around the nucleus with a reddish tinge probably due to blood stain (Figure 2 *j*). The growth spreads as elliptical branching into several segments guided by septum-oriented directions (Figure 2 *d*, *e*, *h*, *j*). Because of their composition and fine inner laminated structure as well as occurrence of decentralized core, the kidney stones can be megascopically and also microscopically classified as whewellite papillary stones[4]. The urinary ionic mineralized product deposition develops its architecture as different concentric layers probably reflecting domains of different urinary conditions. The deposited layers are many times curvilinear (Figure 2 *l*) showing prominent banding (Figures 2 *b*, *h* and 3 *a–g*). The banding width is often variable (20–30 μm) with alternating bands of dark iron stain (Figure 2 *j*), as non-mineralized material with lighter shade of calcium fluorite (CaF_2) (ref. 13). Often, the bands are mixed with clear crystals of CaC_2O_4 and apatite [$Ca_5(PO_4)_3$(OH, F, Cl)] (Figure 2 *j*). After the blood-stained bands, mineralization is largely CaF_2, combined with CaC_2O_4 and eventually merging into CaC_2O_4 in composition alone (Figure 2 *e*).

Interstitial 'Randall's' plaques are formed in response to high urine calcium, and reduced urine volume[3–7]. Subsequently, and for unknown reasons, regions of plaque

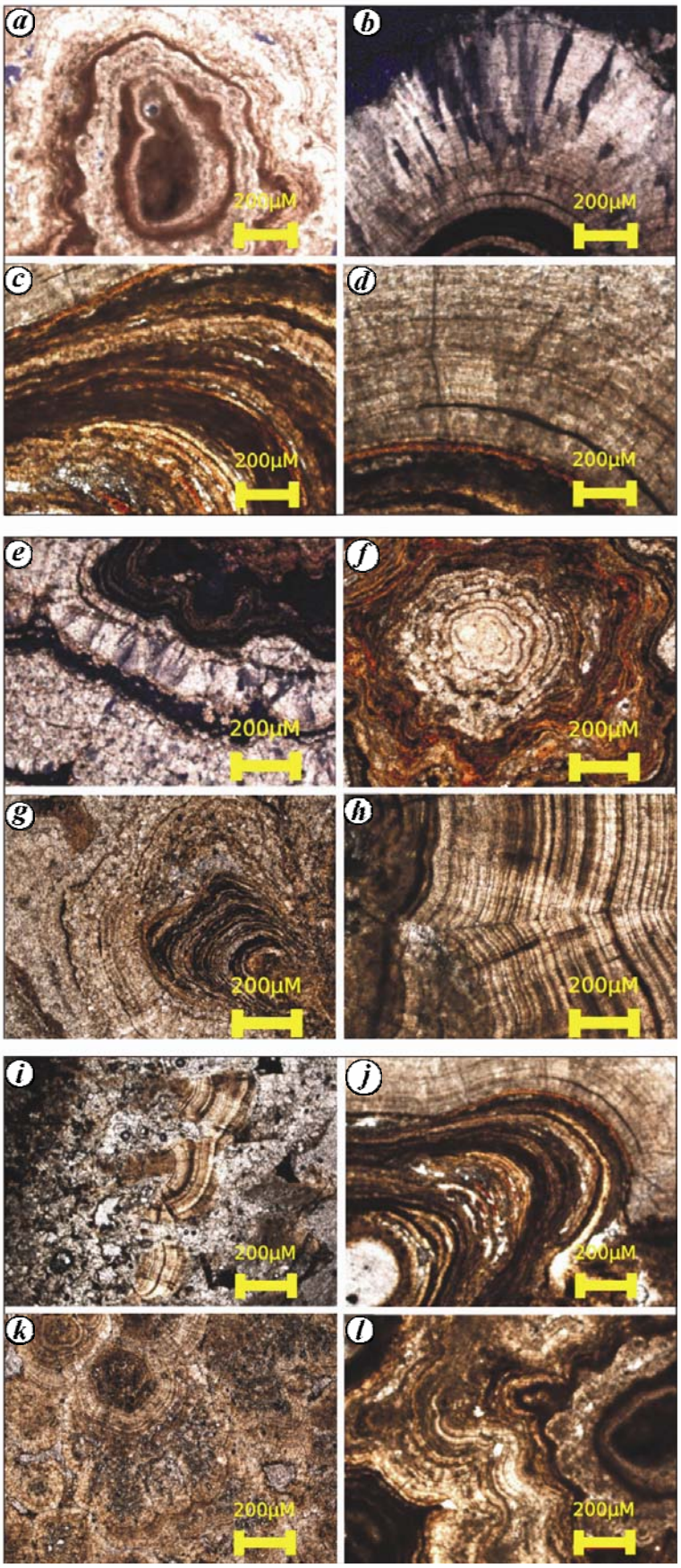

Figure 2 ***a–l.*** Microstructures observed under petrological microscope.

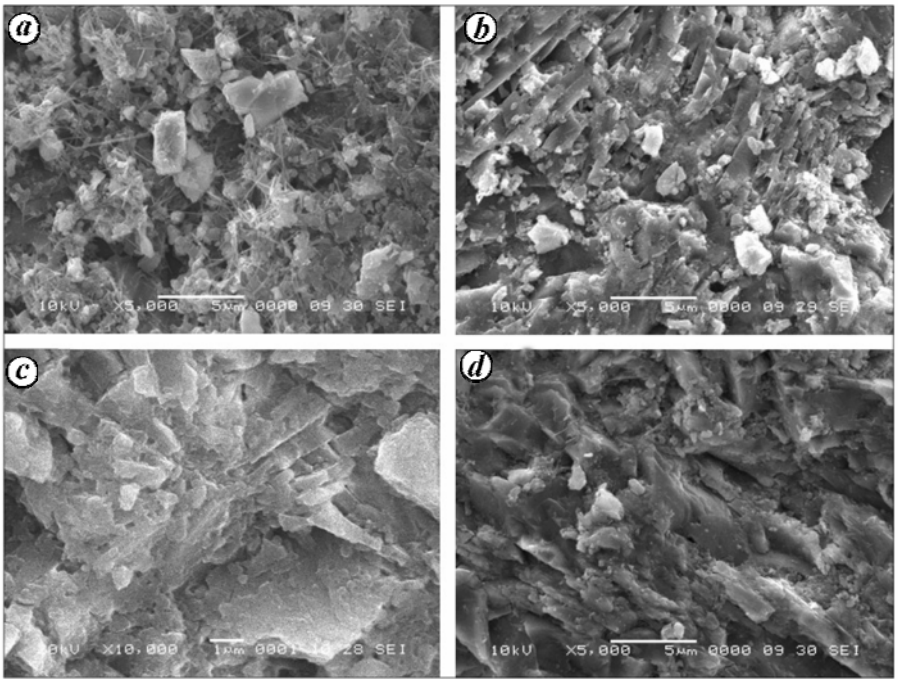

Figure 3 *a–d*. Scanning electron microscopy of uroliths showing different nucleus structures.

are exposed to urine by means of loss of papillary epithelial (urothelial) integrity[3]. Some urine proteins form a layer that covers the exposed plaque; at least in part, this layer contains Tamm-Horsfall protein (THP) and osteopontin, two prevalent urine proteins[1–3] that have affinity for apatite crystals. Within this layer of new matrix, amorphous apatite crystals form, driven by urine super saturations for calcium phosphate species[3–10,12]. Additional urine proteins getting adsorbed to the apatite forming another layer, with repeated bursts of crystallization and coating form the 'ribbon morphology' observed over the tissue plaque. At some point, crystallization is driven by urine super saturation that overcomes the moderating effects of urine proteins and crystals, and extends outward into the urine space and begins to form a stone, as well as successive layers of biological apatite and finally CaC_2O_4 (ref. 4).

Under the optical polarizing microscope in plane-polarized light, strongly few coloured samples of apatite displayed colours corresponding to the specimen colour. Many apatites were found colourless in thin sections, displaying weak to moderate pleochroism. Under the crossed Nicols, colloform, spherulite habit with basal cleavage and poor prismatic cleavage were observed. Parallel extinction, length fast and uniaxial negative interference figure could be identified in large apatite crystals. However, interference figure in small grains was difficult to obtain.

Optical microscopic analysis of urolith was supported by SEM studies by observing the various types of centre which triggers the development of uroliths[10]. In Figure 3 *a*, organic fibres are embedded in CaC_2O_4 matrix and those are observed only in the nidus (nucleus). Laminated sheets of CaC_2O_4 filled with organic matrix are observed in the centre of the urolith (Figure 3 *b*). Radial growth bands are observed in CaC_2O_4 uroliths (Figure 3 *c*). However, outside layers of uric acid urolith are developed by fused matrix of uric acid and not showed any organic crystallization (Figure 3 *d*). From SEM image observations, it is revealed that CaC_2O_4 urolith layers develop around nidus with mixture of inorganic (CaC_2O_4, apatite, CaF_2) and organic (blood stain, 'Randall's' plaques, organic fibres) materials. However, single centred uroliths are made of inorganic constituents, whereas nucleus of inorganic and organic mixture develops multi-centred uroliths.

Our observations under the optical and scanning electron microscope support of uroliths help us to infer, that amorphous apatite forms in the matrix. The biological apatite crystals form toward the stone interior and exterior and likewise depositing CaC_2O_4 which latter process is exclusively of urine origin[3]. Plaque abundance is proportional to urine calcium and inverse to urine volume[7]. The driving forces for plaque and CaC_2O_4 overgrowth are more or less the same. We speculate that the Randall's plaque is amorphous apatite because of the matrix bias of this newly formed material. In other words, the newly formed matrix material (presumed to be urinary proteins) that coats the exposed surface of Randall's plaque has an affinity for apatite crystals, the plaque, or both. Amorphous apatite forms in the urine matrix, perhaps rapidly, and is coated over with urine proteins. Thereafter, perchance more slowly, biological apatite grows in the urine matrix, and is itself over-coated. Finally, CaC_2O_4 and or

more apatite form, and attract matrix, creating the final stone whose overall composition reflects the super saturation present in urine[7].

Apatite plays a key role in the formation of all kidney stones. The crystalline components of the urinary tract are CaC_2O_4, calcium phosphate, struvite, purine or cystine[9]. A majority of urinary stones are admixtures of two or more components, with the primary admixture being CaC_2O_4 and apatite[9]. Fermanor model studies have shown that calcium phosphate nidi are always formed initially and may subsequently become coated with CaC_2O_4 or other components[8].

From micromorphologic studies we show the sequence of steps that lead to the formation of the common human CaC_2O_4 urolith stone and this can be presented in four stages: (1) Formation of a nucleus or a plaque. (2) Uniform concentric rims of blood stain around the nucleus with multiple centres of growth bands. (3) Incremental growth bands of CaF_2 mixed with CaC_2O_4, and calcium phosphate in prominent growth direction forming papillae due to the probable availability of space leading into several papules. The individual growth bands can be ovoid, oblate or elongate, suggesting a driving force of a prominent growth direction and internal available space. (4) Development of radial cracks by the growing nucleus exerting pressure on the mineralized bands, thus resulting in the development of the cracks. Because of the compositional difference between the nucleus and the surrounding zones and the mineralized bands, the tiny papillae are more susceptible to deformation, and get dislocated along the radial cracks (Figure 2 *i*), eventually leading to a complete disruption and destruction of the individual septums, which float in the peripheral mineralized zone (Figure 2 *i*). These floating pieces possibly breakup into smaller pieces that are likely to cause excruciating pain to the kidney-stone patients.

This study is only a preliminary attempt at understanding the microstructure of kidney stones. Detailed research demands meticulous electron microscopic studies on the kidney stones, their chemistry, and the dietary habit and genetics of the patients.

1. Atmani, F., Glenton, P. A. and Khan, S. R., Identification of proteins extracted from calcium oxalate and calcium phosphate crystals induced in the urine forming subjects. *Urol. Res.*, 1998, **26**, 201–207.
2. Devuyst, O., Dahan, K. and Pirson, Y., Tamm–Horsfall protein or uromodulin: new ideas about an old molecule. *Nephrol. Dial. Transplant.*, 2005, **20**, 1290–1294.
3. Evan, A. P. *et al.*, Mechanism of formation of human calcium oxalate renal stones on Randall's plaque. *Anat. Rec.*, 2007, **290**, 1315–1323.
4. Giannosi, M. L., Mongelli, G. and Summa, V., The mineralogy and internal structure of kidney stones. *NDT Plus*, 2009, **2**, 418–419.
5. Hyacinth, P., Rajamohanan, K., Marickar, F. Y. M., Koshy, P. and Krishnamurthy, S., A study of ultra structure of urinary calculi by scanning electron microscopy. *Urol. Res.*, 1984, **12**, 227–230.
6. Kumar, N., Singh, P. and Kumar, S., Physical, X-ray diffraction and scanning electron microscopic studies of urolith. *Indian J. Biochem. Biophys.*, 2006, **43**, 226–232.
7. Kuo, R. L. *et al.*, Urine calcium and volume predict coverage of renal papilla by Randall's plaque. *Kidney Int.*, 2003, **64**, 2150–2154.
8. Leusmann, D. D. and Sabinski, F., Potential contribution of optional urease-positive bacteria to idiopathic urinary calcium stone formation. II. Microlith formation kinetics in a fermenter model of the urinary tract infected by optional urease-positive microorganisms. *Urol. Res.*, 1996, **24**, 73–78.
9. Mandel, N., Mechanism of stone formation. *Sem. Nephrol.*, 1996, **16**, 364–374.
10. Maragos, P., Sofou, A., Stamou, G. B., Tzouvaras, V., Papatheodorou, E. and Stamou, G. P., Image analysis of soil micromorphology: feature extraction, segmentation, and quality inference. *EURASIP J. Appl. Signal Process.*, 2004, **6**, 902–912.
11. Rez, P., Fong, H. and Sarikaya, M., Scanning electron microscopy and atomic force microscopy of the ring structures in human calcium oxalate urinary stones. *Microsc. Microanal*. (*Suppl. 2*), 2002, **8**, 746CD–747CD.
12. Parks, J. H., Coward, M. and Coe, F. L., Correspondence between stone composition and urine supersaturation in nephrolithiasis. *Kidney Int.*, 1997, **51**, 894–900.
13. Sai Satish, R., Ranjit, B., Ganesh, K. M., Rao, G. N. and Janardhana, C., A quantitative study on the chemical composition of renal stones and their fluoride content from Anantapur District, Andhra Pradesh, India. *Curr. Sci.*, 2008, **94**(1), 104–109.

ACKNOWLEDGEMENTS. We thank the Head, Department of Geology, University of Pune, Pune for providing facilities. We also thank DST and UGC, New Delhi for providing FIST and DRS (SAP) funds for infrastructure. The help rendered by Prof. N. R. Karmalkar in microscopic studies is acknowledged. S.S.K. thanks UGC, New Delhi for funds to carry out this work.

Received 2 February 2010; revised accepted 27 October 2010

Carbon storage and sequestration in bamboo-based smallholder homegardens of Barak Valley, Assam

Arun Jyoti Nath and Ashesh Kumar Das*

Department of Ecology and Environmental Science,
Assam University, Silchar 788 011, India

Smallholder farming systems throughout the world are believed to be potential sinks to remove atmospheric CO_2. Smallholder bamboo farming system in Barak Valley, Assam, which forms a part of the traditional homegarden system, holds promise in this respect. Occurrence of bamboo in all homesteads coupled with progressive increase in culm density over the years reflects its potential for carbon (C) storage. Hundred homegardens were selected from the study site and the total number of culms from all the different age classes per clump of *Bambusa cacharensis*, *Bambusa vulgaris* and *Bambusa balcooa* were recorded with their diameter at breast height. Harvest method was employed to estimate the aboveground biomass

*For correspondence. (e-mail: asheshdas684@hotmail.com)